Asia-Pacific Journal of Science and Technology: Volume: 28. Issue: 06. Article ID.: APST-28-06-16. Research Article

APST

Asia-Pacific Journal of Science and Technology

https://www.tci-thaijo.org/index.php/APST/index

Published by the Research and Graduate Studies Division,
Khon Kaen University, Thailand

Discrete element analysis of density dependency of granular materials under different directions of true triaxial cyclic loading

Daraporn Phusing[1,*], Korchoke Chantawarangkul[2] and Pulpong Pongvithayapanu[1]

[1]Department of Civil Engineering, Faculty of Engineering at Sriracha, Kasetsart University Sriracha Campus, Chonburi, Thailand
[2]Department of Civil Engineering, Faculty of Engineering, Kasetsart University, Bangkok, Thailand
[*]Corresponding author: daraporn@eng.src.ku.ac.th

Received 3 January 2022
Revised 3 November 2022
Accepted 6 November 2022

Abstract

This paper introduces the macro and micro response behaviors of dense, medium, and loose samples of granular materials where the initial void ratio e_o was 0.57, 0.67, and 0.73, respectively, under five different directions of true triaxial cyclic loading tests using the discrete element method (DEM). The experimental results with similar cyclic stress paths were applied to validate the DEM results. The results showed variations in the principal stress-strain relationship as well as the strain increment vector of each sample in the 1st and 5th cycles. There was a qualitative similarity between the strain increment vectors for the experimental results and the DEM. The micro response analysis indicated that there were substantial differences in the coordination number as well as the sliding contact fraction of all samples under different directions of cyclic testing. At the macro-micro level, the stress ratio and fabrics of the strong contact forces presented strong unity even under different directions of the cyclic principal stresses, which increased with the number of cycles. However, there was only one weak unity for the different levels of density.

Keywords: Cyclic loading, Density, DEM, Granular materials, True triaxial loading

1. Introduction

Granular materials have been used to explore behavior under triaxial cyclic loading in several experiments as well as in numerical simulation studies. The discrete element method (DEM) is a well-known theory in geotechnical engineering for granular soil simulation. In many cases, cyclic stresses are arranged in compression and extension loading with the same amplitude [1-11]. For example, Nakai et al. [5] conducted experiments with Toyoura sand under various drained cyclic true triaxial loading stresses with three different directions of principal stresses. They found that the shear strain increment and relationship between stress and dilatancy were completely changed by the stress paths. In addition, the volume contraction was not substantial, even with a change in the principal stress axes, when the stress path did not change. Phusing and Suzuki [11] used DEM [12] to generate a medium-dense sample of granular materials and sheared the sample under four different cyclic stress paths repeated in five cycles, similar to Nakai et al. [5], to explore the macro behavior and micromechanical responses. Their study found similar trends for the stress and strain as well as dilation in the results of the experiment and the DEM. Furthermore, the single relationship among the stress ratio, the fabric of all normal and strong contact was not dependent on the cyclic stress paths when considering only the strong contact or the number of cycles.

For granular soil density, several studies have been conducted using cyclic load testing, but the reported results were different. O'Sullivan et al. [7] achieved different strain amplitudes of strain-controlled cyclic triaxial tests to analyze macro mechanic and micro reacts of granular materials. It was reported that the cyclic behaviors of granular materials could be created by the DEM. According to Hu et al. [8], the cyclic tests' amplitude could affect both the accumulation of strain and the development of fabric structure anisotropy of sand. In addition, Jiang et al. [13] simulated two different initial relative densities of granular materials under different cyclic amplitudes and an average shear stress. Microstructure evolutions were reported, and the study concluded that the

coordination number and contact fabric were dependent on the relative density and cyclic stress, with no clear relationship between the normal contact and the stress ratio. However, there was a relationship between the strong contact and the stress ratio.

Several studies using samples with different levels of density were tested under the limitation of stress paths (compression and extension cyclic tests with a constant amplitude). Thus, the model accuracy under general stress conditions with different amplitudes must be certified to analyze the soil dynamic behavior, such as liquefaction phenomena. Otsubo et al. [14] used DEM to simulate cyclic instability followed by liquefaction and reported that loose samples had a large rate of inherent anisotropy because a sample with initial anisotropy tends to increase the deformation more in a weaker direction, causing lower liquefaction resistance' a sample with an isotropic fabric potentially exhibited the greatest liquefaction resistance. In addition, different sample preparation methods induced different degrees of inherent anisotropy in soil samples [15-17]. In terms of microstructure, researcher have explained that the different initial anisotropic properties of granular soils lead to different fabric tensors, and that they affect the level of the stress ratio at the critical state [18-22]. To avoid the effect mentioned, the current study used spheres to create the initial isotropic assembly to explore the fundamental effect of density on mechanical behavior where the complicating effect of particle shape has been removed. However, this study limited the maximum stress ratio for all the specific cyclic stress paths and used spherical particles in different densities samples. The study used these limits because it aimed to research the mechanical behavior found in granular materials under similar amplitudes of cyclic loading at different densities by using similar shapes of particles to obtain a lower level of anisotropy. Furthermore, the sample was sheared under several kinds of drained cyclic true triaxial stress paths by using a low stress and creating small strain behavior.

A medium-dense sample under various amplitudes cyclic loading has been studied in other experiments and simulations [5,11], focusing on the behaviors of loose and dense samples with various amplitudes. However, there has been no report on differences in density behaviors. To serve the purpose mentioned, the current study aimed to determine the behavior of density-dependent granular materials under different directions of true triaxial cyclic stress, to investigate macro behavior, and report the micromechanical response influenced by the density. The initial isotropic samples (loose, medium, and dense) were tested under 5 imposed cyclic stress paths, using a stress-controlled method. The controlled stress was selected to control the sample with an initial isotropic compression 100 kPa before shearing. Then, the imposed cyclic true triaxial stress paths were tested (using 100 kPa constant mean stress). However, the initial anisotropic condition was not considered in this study. The Oval DEM software, [23] was used to investigate the different densities of granular samples and directions of the cyclic true triaxial stress paths under both 100 kPa constant mean stress and stress-controlled conditions.

2. Materials and methods

2.1 Discrete element method theory

The DEM was first created by Cundall and Strack [12]. The governing equation of DEM is expressed in a matrix form as Equation (1):

$$M\Delta\ddot{X} + C\Delta\dot{X} + S\Delta X = \Delta F \tag{1}$$

where M is the mass matrix, ΔX is the incremental displacement vector, including incremental rotations, C is the damping matrix, S is the stiffness matrix, and ΔF is the incremental force vector, including incremental moments. Using the governing equation, the equilibrium is set for resultant forces and moments at the center of each particle. In each incremental time, the displacement and rotational angle of each particle are calculated. Further information on DEM is available in [12]. The free computer program for DEM named Oval [23] was used in this study. The inter-particle friction coefficient as well as the rotational and translational damping were used.

2.2 Sample preparation

The diameters of the spheres were 3-4.5 mm, as formed by Sazzard et al. [11]. Figure 1 shows the gain size distribution curve, where $d_{min} = 3$ mm., $d_{max} = 4.5$ mm. and $d_{50} = 3.7$ mm. Figure 2(A) shows that the center of each particle was placed in the position spacing 5 mm, with 20 spheres in each dimension, producing 8,000 spheres in a cubic sample. The isotropic sample was created by compressing the initial scant sample all around using the periodic boundary to remove the effect of boundary. Then, the sample was isotropically compressed with a confining pressure of 100 kPa. To create the loose, medium, and dense samples in isotropic compression, the coefficient of interparticle friction μ was assigned as 0.5, 0.2, and 0, respectively. A stress rate of $1x10^6$ Pa/sec was used up to a maximum pressure of 100 kPa. The sample data before shearing are presented in Table 1 and figures of all samples before sharing are shown in Figure 2 (B-D). The DEM input parameters for mass density ρ was 2,650

kg/m^3, with a stress rate of $2x10^6$ Pa/sec for shearing. Both normal stiffness (k_n) and tangential contact stiffness (k_s) were 1×10^6 N/m. Both the rotational damping C_r and translational damping C_t were 0.05. The time step increment Δt was 1×10^{-6} sec.

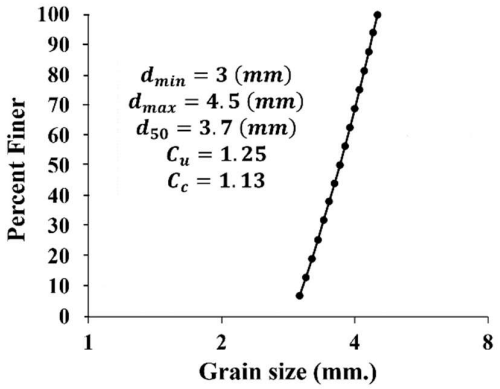

Figure 1 Graph of gain size distribution curve.

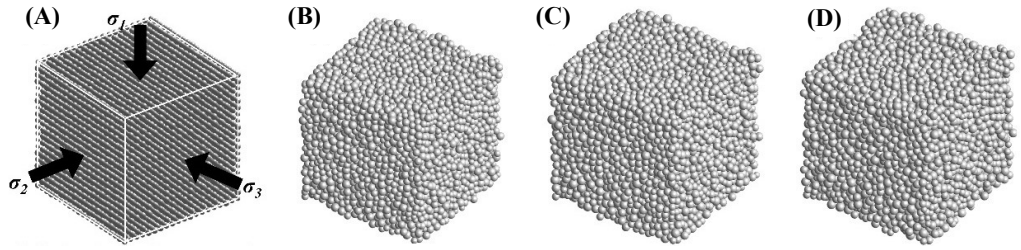

Figure 2 Samples before isotropic (A) compression; (B) loose; (C) medium; and (D) dense.

Table 1 Sample data before shearing.

Sample type	Inter-particle friction coefficient (μ)	Void ratio	Size of cubic sample (cm)
Loose	0.5	0.73	$7.3 \times 7.3 \times 7.3$
Medium	0.2	0.67	$7.2 \times 7.2 \times 7.2$
Dense	0	0.57	$7.1 \times 7.1 \times 7.1$

2.3 Simulation programs

Five different directions of cyclic stress paths were conducted, called Test 1, Test 2, Test 3, Test 4, and Test 5. They were plotted as projections on the normalized π-plane, as seen in Figure 3 (A-E). In the figures, all five stress paths started at the last stresses of isotropic compression where σ_1, σ_2, and σ_3 are 100 kPa (Point A). Later, the sample was sheared, following the directions of stress paths as shown in Figure 3. In Test 1 (Figure 3 (A)), the sample was sheared from point A where $\sigma_1 = \sigma_2 = \sigma_3 = 100$ kPa until $\sigma_1/\sigma_3 = 1.24$ and turned in the direction of a triangular figure in a counterclockwise direction ①-②-③ for 5 cycles and then the direction was reversed to the clockwise direction ③-②-① for 5 more cycles. In Test 2 (Figure 3 (B)), the sample was subjected to the first loading and unloading where the major stress changes from direction σ_1 to σ_2 and σ_3, following steps ① to ⑥. In Test 3 (Figure 3 (C)), a triaxial compression and extension following step ① to ⑫ was applied to the sample. For Test 4 (Figure 3 (D)), the sample was tested according to Mohr-Coulomb's criterion using stages ① to ⑥ for 5 cycles. For the final stress path in Test 5 (Figure 3 (E)), the sample was tested by triaxial loading and unloading from point A to $\sigma_1/\sigma_3 = 1.24$ and repeated following steps ① to ② for 10 cycles; then, the direction was changed in step ③ to ④, where the principal stress deformed from σ_1 to σ_3 for 10 more cycles. Next, the direction was reversed in step ⑤ to ⑥ for 5 more cycles and continued in step ⑦ to ⑧ for 5 more cycles. For all tests, the maximum and minimum principal stresses were $\sigma_{maximum} = 1.159$ kPa and $\sigma_{minimum} = 0.935$ kPa, respectively. The maximum principal stress axis changed from the vertical axis 1 to the horizontal axes of 2 and 3, respectively. The vertical axis 1 direction is the maximum while the horizontal 2 and 3 axes were the minimum. At the same time, if the horizontal 2 axis was the maximum, then vertical 1 and horizontal 3 were the minimum axes. However, if horizontal 3 was the maximum, then vertical 1 and horizontal 2 were the minimum. Figure 4 (A-C) show that the mean stress p against the

deviatoric stresses q and p was constant during shearing, with q and p described in Equations (2) and (3), respectively.

$$q = \sqrt{\frac{1}{2}\{(\sigma_1 - \sigma_2)^2 + (\sigma_2 - \sigma_3)^2 + (\sigma_1 - \sigma_3)^2\}} \quad (2)$$

$$p = (\sigma_1 + \sigma_2 + \sigma_3)/3 \quad (3)$$

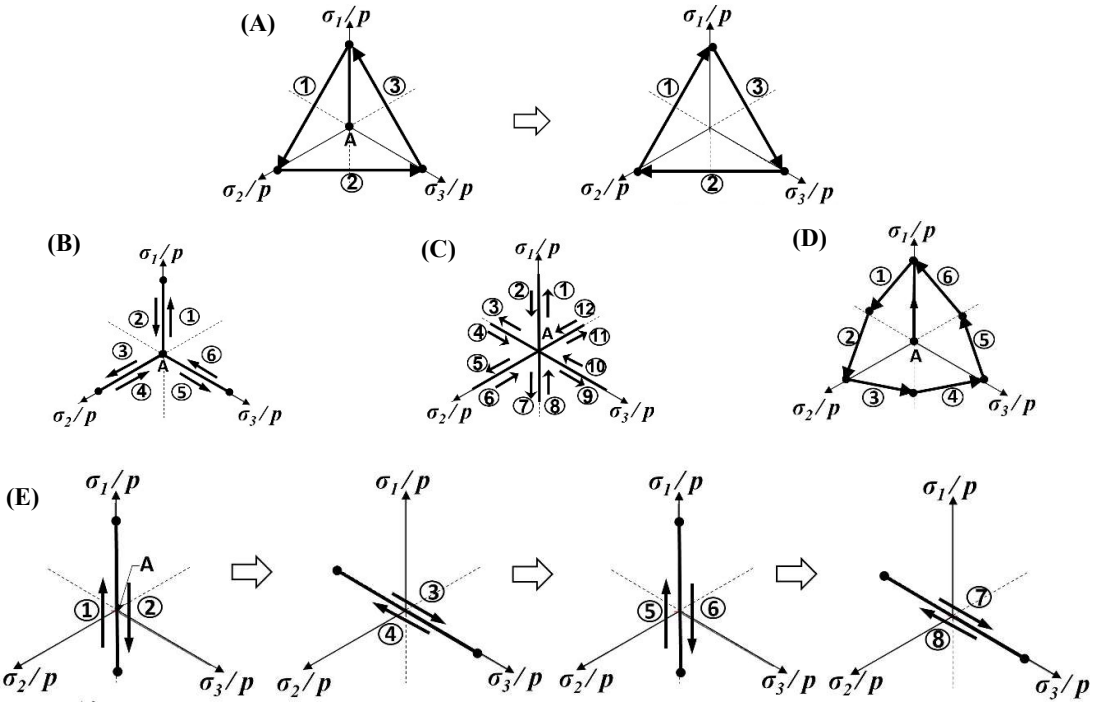

Figure 3 Simulation program projections on normalized π-plane of (A) Tests 1, (B) Test 2, (C) Test 3, (D) Test 4 and (E) Tests 1-5.

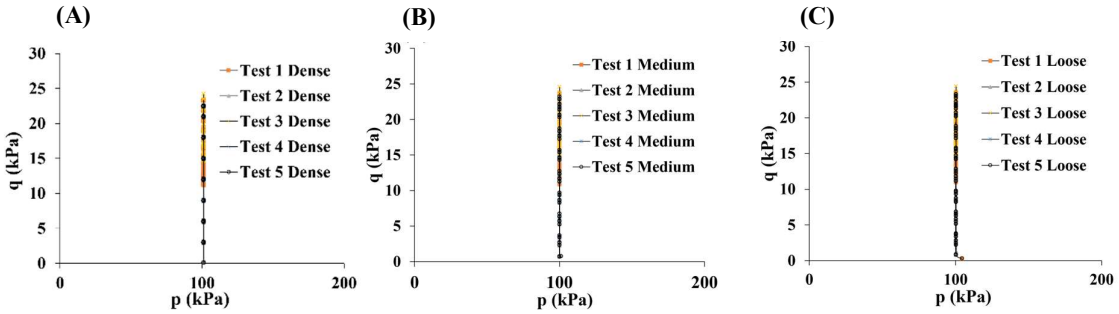

Figure 4 Graph of relationship between stress q against mean stress p of all tests for (A) dense, (B) medium, and (C) loose sample.

3. Results

3.1 Stress-strain relationship

Figures 5 (A-C) indicate the evolution of the equivalent deviatoric strain ε_d (%) and volumetric strain ε_v by increasing the stress ratio q/p and σ_1/σ_3 of the loose, medium, and dense samples, respectively, under 5 cycles of Tests 1, 2, and 3. The equivalent deviatoric strain ε_d is defined in Equation (4) while the volumetric strain ε_v is defined in Equation (5).

$$\varepsilon_d = \sqrt{\frac{2}{3}\{(\varepsilon_1 - \varepsilon_2)^2 + (\varepsilon_2 - \varepsilon_3)^2 + (\varepsilon_1 - \varepsilon_3)^2\}} \quad (4)$$

$$\varepsilon_v = dv/v = (\varepsilon_1 + \varepsilon_2 + \varepsilon_3)/v \quad (5)$$

where dv is the volume change, v is the initial sample volume at the beginning of shearing, ε_1, ε_2, and ε_3 are the vertical strain in direction 1 and the horizontal strains in directions 2 and 3 (Figure 2A).

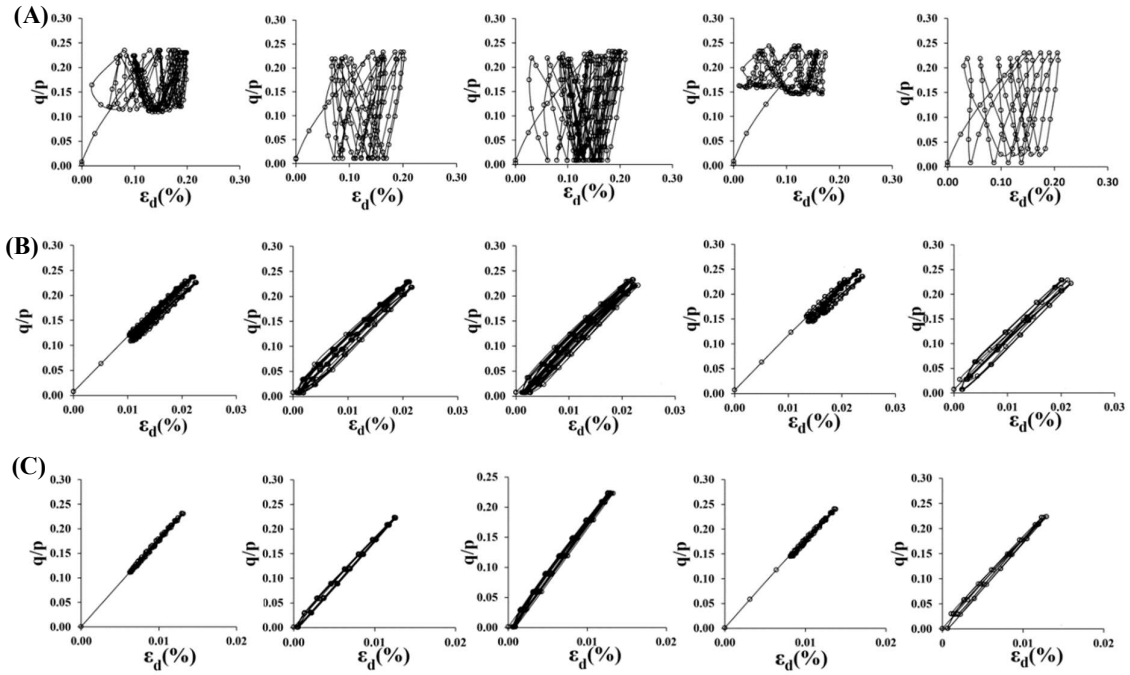

Figure 5 Graph of relationship between q/p and ε_d of (A) loose, (B) medium, and (C) dense samples for 5 cycles of all tests.

Figures 5 (A-C) shows that the stress-deviatoric strain relationships for the loose sample for those tests were strongly influenced by the stress path. However, the relationships for the medium and dense samples were not changed by the stress path. This result indicated that the stress-deviatoric strain relationship differed, depending on the density of the sample as well as the direction of cyclic loading. In addition, the stress-deviatoric strain did not depend on the number of cycles.

Figures 6 (A-C) show the relationship between ε_v (%) against σ_1/σ_3 under 5 cycles of Tests 1, 4, and 5 and ε_v (%) against the stress ratio q/p that was used for Tests 2 and 3 for the loose, medium, and dense samples, respectively. The stress ratio q/p was used for Tests 2 and 3 because the stress ratio σ_1/σ_3 in those tests did not change, where $\sigma_1 = \sigma_3$. Figures 6 (A-B) show that the volumetric strains ε_v of the loose (Figure 6A) and medium (Figure 6B) examples were compressed substantially in the initial states, which later decreased and became almost stable after a few cycles. In addition, changing the direction of the major principal stresses in the cyclic loading caused the volumetric stress to behave similarly to its initial state, which was not influenced by the cyclic stress history. This has been reported in the experimental results for medium dense sand by Nakai et al. [5]. For the dense sample, shown in Figure 6 (C), there was rarely accumulated volumetric change. In addition, Figures 6 (A-B) show that the volumetric strain was strongly influenced by the different directions of the cyclic loading stress path. Figure 6 (A) shows that the maximum volumetric strain of the loose sample after 5 cycles was approximately 1% for all tests. However, in Figure 6 (B), the volumetric strain of the medium sample in Test 3 reached its maximum after 5 cycles, whereas Test 4 had the minimum. This result was mentioned by Phusing and Suzuki [11] using DEM. For the dense sample in Figure 6 (C), the volumetric strains in all tests were in a stable state. These volumetric strains differed depending on the stress path but did not change much after the 5th cycle. It can be observed that the stress-volumetric strains for the different density levels of granular materials were not influenced by the number of cycles.

Figures 7 (A-C) show the evolution of volumetric strain ε_v with the number of cycles for all density samples under all tests. The volumetric strain increased together with the number of cycles in the loose and medium sample

(Figures 7A-B) in all tests except for the dense sample (Figure 7C). Additionally, in Figure 7 (A), the volumetric strain in Test 3 increased according to the number of cycles more than in the other tests, whereas in Test 5 it increased the least. The reason reported by Phusing and Suzuki [11] was that Test 3 had a higher degree of unusuality than the other tests, and the degree of unusual cyclic stresses might cause the expansion of both the deviatoric strain and volume. The report of an unusual degree of cyclic stress paths leading to volume expansion of the granular soil was mentioned by Nakai et al. [3]. As a result, the current study concluded that the volumetric strain differed based on the direction of the cyclic stress path and number of cycles in the loose and medium samples but was independent on these parameters in the dense sample. Furthermore, the evolution of volumetric strain of the granular materials under true triaxial cyclic loading differed based on the initial void ratio and number of cycles as well as the degree of unusual cyclic stress paths.

Figures 8 (A-C) show the graph between the ε_v (%) and σ_1/σ_3 in Test 5 from all samples in the total of 30 cycles (Figure 3E). Figure 8 (A) shows that the volumetric strain of the loose sample was much extended in the 1st cycle, that it was steady after a few cycles until the 10th cycle (steps ①-②) and increased when changing the direction of the principal stress before continuing in a steady state until the next 10th cycle (steps ③-④). Then, the sample was reloaded cyclically for the next 5 cycles and 5 more cycles (steps ⑤-⑥-⑦-⑧), where the stress path was the same as before. There was no substantial change in the cumulative volumetric strain. Even though the major principal direction had changed, the stress paths remained the same. For the medium sample in Figure 8 (B), the volumetric strain had some characteristics similar to the loose sample, but it accumulated rapidly and entered a steady state under cyclic loading by changing the principal stress direction and had similar stress experience. In Figure 8 (C), the dense sample was compressed and stabilized for the first 10 cycles. The compression increased when changing the principal stress direction. The number of cycles had no influence on the dense sample.

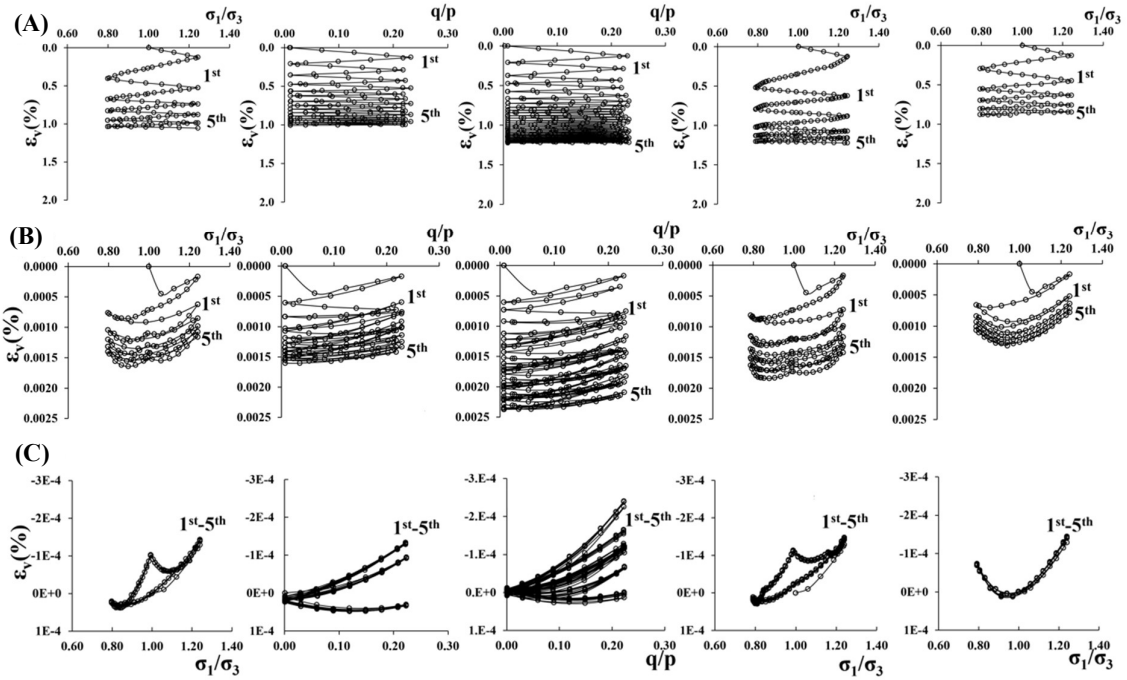

Figure 6 Graphs of ε_v and σ_1/σ_3 for Tests 1, 4, and 5 and of q/p for Tests 2 and 3 of (A) loose, (B) medium, and (C) dense samples for 5 cycles in all tests.

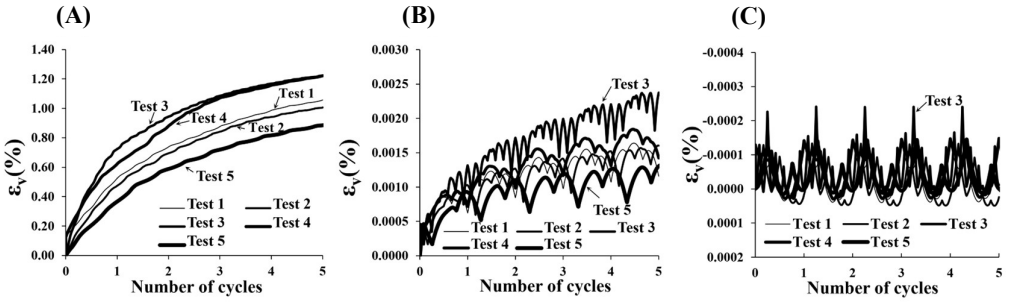

Figure 7 Graphs of ε_v and number of cycles of (A) loose, (B) medium, and (C) dense samples in 5 cycles of all tests.

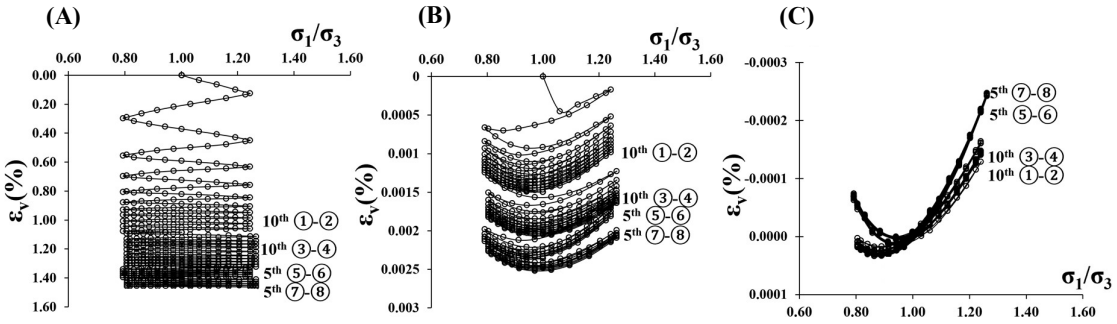

Figure 8 Graphs of ε_v and σ_1/σ_3 of (A) loose, (B) medium, and (C) dense samples in Test 5.

3.2 Strain increment vectors

Figures 9 (A1-C2) show the 1st and 5th cycles of the strain increment vectors on the normalized π plane by mean stress p for Tests 1, 2 and 4 of the loose and dense samples. The results of the medium and dense samples were similar. Thus, the results of the loose and dense were selected for discussion in this section. It can be seen from Figure 9 that the strain increment directions were changed greatly by the stress path directions of the loose and dense samples. Figures 9 (A1-A2) show the directions of the strain increment vectors of the loose sample for the 1st and 5th cycles in Test 1. The strain increment vectors in the 1st cycle of the loose sample were far from the stress paths but they came closer in the 5th cycle. This can be seen in Test 4 (Figure 9C1-C2) too. In Figures 9 (A2, B2, C2), the direction of the strain increment did not depend on the number of cycles in any tests of the dense sample. Thus, it was concluded that the directions of strain increment depended on the number of cycles of the loose sample. Furthermore, the strain increment vectors differed depending on the density under true triaxial cyclic stresses.

3.3 Microscopic response

The micro data of coordination numbers and sliding contact fractions [23,26] were defined as equation (6) and (7), respectively:

$$\text{Coordination number} = (2 \times N_c)/N_p \tag{6}$$

$$\text{Sliding contact fraction} = (N_s/N_c) \times 100\ (\%) \tag{7}$$

where N_c is the number of contacts, N_s is the number of sliding contacts, and N_p is the number of particles.

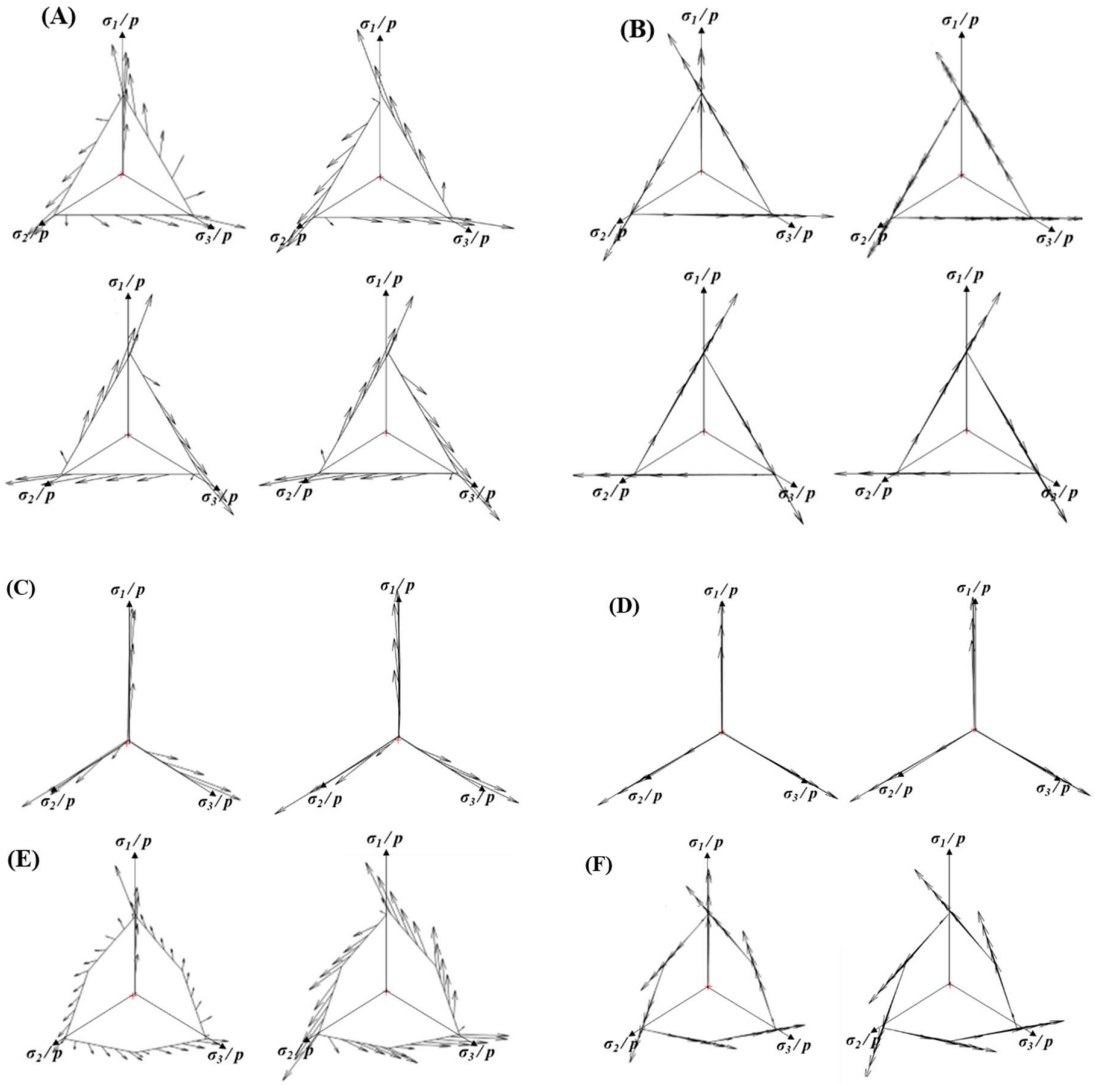

Figures 9 Strain increment vector directions in 1st and 5th cycles on normalized π plane of (A) loose Tests 1, (B) dense Test 1, (C) loose Test 2, (D) dense Test 2, (E) loose Test 4 and (F) dense Test 4 samples.

Figure 10 presents the relationship of coordination numbers with the number of cycles and Figure 10 presents sliding contact fractions for the loose, medium, and dense samples in all tests. The coordination number of the dense sample before shearing was 5.94, while the medium and the loose sample values were 4.88 and 4.09, respectively. The coordination number of the dense sample was greater than those for the medium and loose samples. Figure 10 shows that the coordination number of the loose sample gradually decreased with an increased number of cycles. The medium sample also showed a slight decrease, whereas the dense sample was independent of the number of cycles. There was a similar tendency with the sliding contract fraction for the loose sample shown in Figure 11. However, the medium and dense samples did not produce changes in their sliding contract fractions when the number of cyclic loadings increased. It seemed that the coordination numbers as well as the sliding contract fractions for all samples had little influence on changing the direction of the cyclic tests (Tests 1-5). The conclusion from this study was that coordination numbers as well as sliding contract fractions depended on the density and cyclic stress paths. The reduction in the coordination numbers with increasing void ratios was similar to the trend from the DEM simulations reported by [6,27].

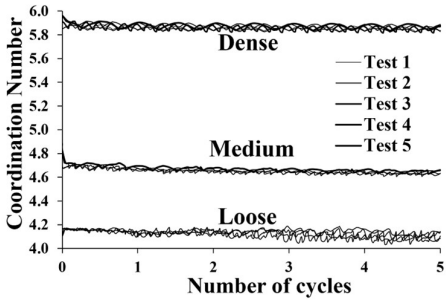

Figure 10 Coordination number against number of cycles of loose, medium, and dense samples of all tests.

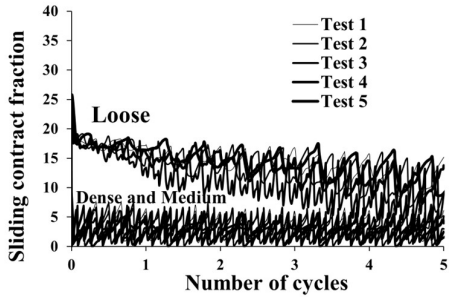

Figure 11 Graph of sliding contact fraction versus number of cycles of loose, medium, and dense samples of all tests.

3.4 Macro and micro relationships

The macro scale behavior and micro data under various true triaxial cyclic loadings are discussed in this section. Figures 12 (A-C) show the relationship between the macro behavior represented by q/p and the fabric ratio in all F_d/F_m. Figure 13 shows F_d^s/F_m^s of the dense, medium, and loose samples in all cyclic tests in 5 cycles. The normal contact vectors were produced by all contacts in all directions of the major, intermediate, and minor contacts as F_{11}, F_{22}, and F_{33} and by the directions F_{11}^s, F_{22}^s, and F_{33}^s. equation (8) by Satake [28] defines the unit vector for all normal contacts whereas equation (9) by Kuhn [10] defines the unit vector of the strong contacts:

$$F_{ij} = \frac{1}{N_c}\sum_{k=1}^{N_c} n_i^k n_j^k \qquad i,j = 1,2,3 \tag{8}$$

$$F_{ij}^s = \frac{1}{N_c}\sum_{s=1}^{N_c^s} n_i^s n_j^s \qquad i,j = 1,2,3 \tag{9}$$

where N_c is the number of contacts, N_c^s is the number of strong contacts, n_i^k is the part of the unit vector n_k at each contact, and n_j^s is the part of n_s as the strong contact force in each unit. When a contact force is larger than f_{ave}^n on average, it is classified as a strong contact force. Equation (10) shows the average contact force:

$$f_{ave}^n = \frac{1}{N_c}\sum_{i=1}^{N_c} f_i^n \qquad i,j = 1,2,3 \tag{10}$$

where f_i^n is a normal contact force. Figures 12 (A-C) show that the macro and micro relationships of all contacts differed depending on the cyclic stress paths as well as the density. However, the dense and medium samples were independent of the number of cycles, as shown in Figure 12 (A-B), whereas the loose sample were dependent on the number of cycles, as shown in Figure 12 (C).

The macro-micro relationship shows unity when considering strong contacts (Figures 13 A-C) whereas the weakness unity was observed when considering all contacts (Figures 12 A-C). The unity of the macro-micro relationship of strong contacts under monotonic loading testing has been reported [6,29-31]. For example, Liu et al. [31] selected isotropic samples with different densities and sheared until reaching the critical state under various monotonic intermediate principal stress ratios (b values). Their study found that the total fabric and strong fabric components showed the same variation trends as b values but were wholly different in weak fabrics., Salimi et al. [32]

developed the coupled fluid-discrete element method to test an initial anisotropic sample under undrained true triaxial loading, finding that the loose sample was rotten due to movement instability. Then, it was shown that stress ratio, mobile friction angle, and pore water pressure at the beginning of instability depend on the lode angle (in the case of an intermediate principal stress ratio). In addition, Ng [33] indicated that the stress ratio σ_1/σ_3 was more correlated with the normal contact force than with the unit normal contact force in several stress paths.

Regarding the cyclic loading tests, Antony et al. [29] reported that the stress ratio to the square root of the fabric ratio contributed by the strong contacts was ≈ 0.5 whereas Sazzard and Suzuki [6] reported different values of q/p to F_d^s/F_m^s (that is ≈1), regardless of the sample density. However, in the current study, Figures 13 (A-C) show that the results of q/p to F_d^s/F_m^s of the loose, medium, and dense samples of all tests were all ≈1. Figure 14 is a combination of Figures 13 (A-C), showing that there was weak unity in the strong contacts under the different densities. Elastic components might be either ignored in this case or might have a large influence on cyclic loading.

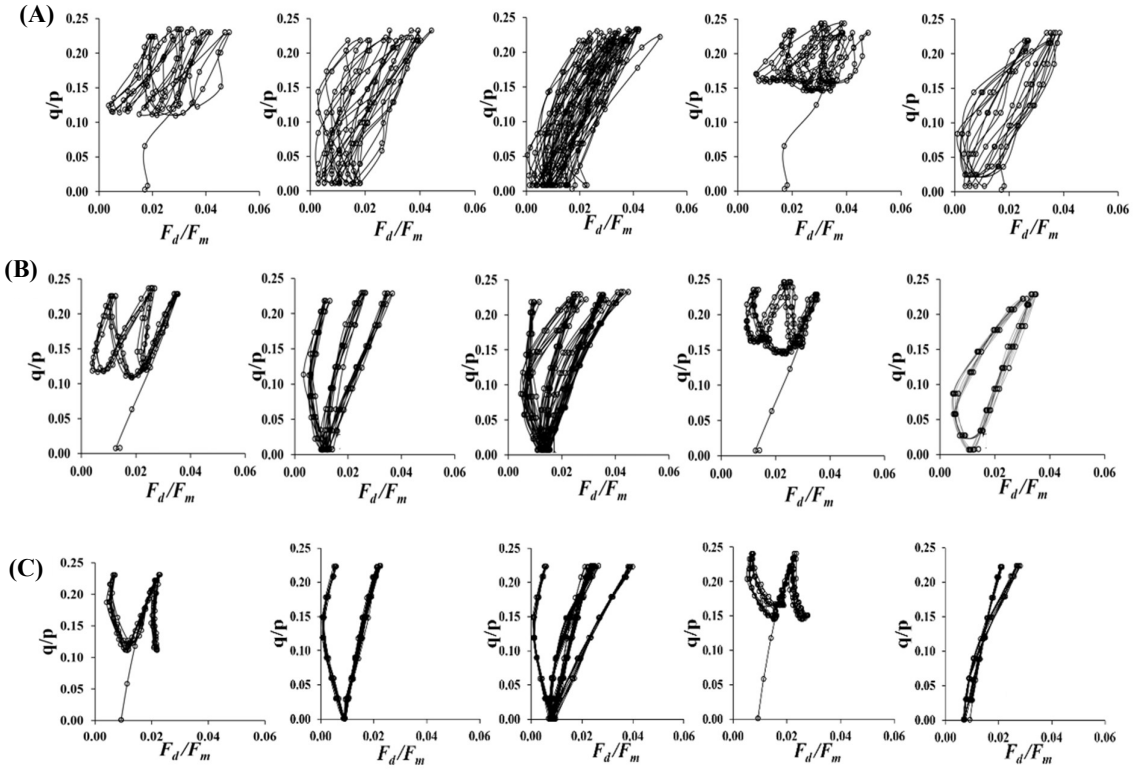

Figure 12 Graphs of stress ratio against deviatoric fabric ratio of F_d/F_m in (A) loose, (B) medium, and (C) dense samples for all cyclic tests in 5 cycles.

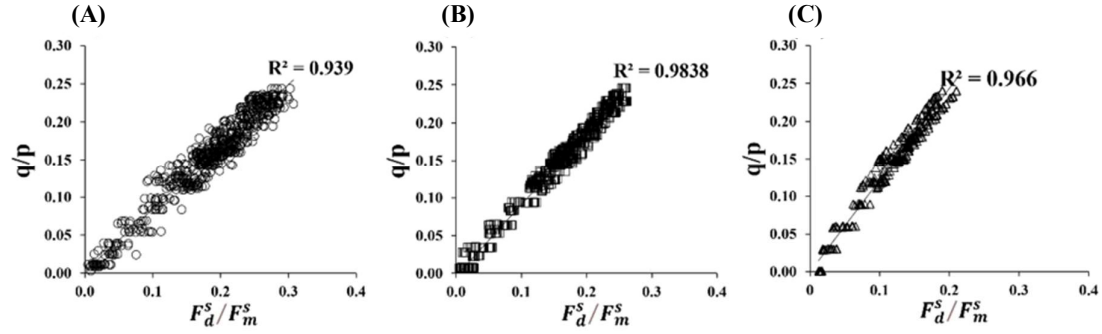

Figure 13 Graphs of stress ratio against deviatoric fabric ratio in F_d^s/F_m^s for (A) loose, (B) medium, and (C) dense samples for all cyclic tests in 5 cycles.

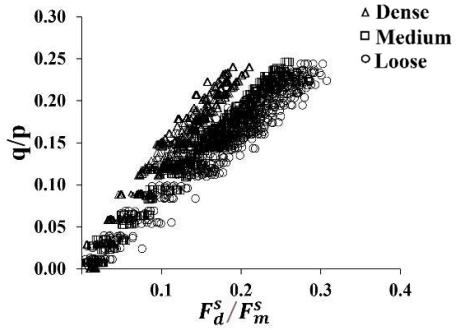

Figure 14 Graph of combination of samples for all cyclic tests in 5 cycles.

4. Conclusion

The DEM method produced good results regarding the real behavior of granular soil under different directions of cyclic loading. Directions of strain increment were influenced by the number of cycles of the loose sample but were independent of this in the dense and medium samples. Additionally, the volumetric strain increased according to the number of cycles of the loose and medium samples but not for the dense sample. Unique macro and micro relationships occurred when strong contacts were considered for all levels of density. However, for the strong contact, the relationship of macro and micro behavior showed no unity.

5. Acknowledgements

The authors would like to thank the Faculty of Engineering at Sriracha, Kasetsart University Sriracha campus, Thailand for kind support regarding experimental instruments used in this study, such as the Matlab program.

6. References

[1] Tatsuoka F, Ishihara K, Drained deformation of sand under cyclic stresses reversing direction. Soils Found. 1974;14(3):51-65.

[2] Pradhan Tej BS, Tatsuoka, F, Sato, Y. Experimental stress-dilatency relations of sand subjected to cyclic loading. Soils Found. 1989;29(1):45-64.

[3] Nakai T, Hiroshikawa T, Korenaka, Hinokio M, editoes. Elasto plastic model for sand under cyclic loading. Third Asia-Pacific Symposium on Advances in Engineering Plasticity and its Applications. 1996 Aug 21-24; Hiroshima, Japan. Amsterdam: Elsevier; 1996.

[4] Nakai T, Hinokio M, Hiroshikawa T, Yoshida H, editors. Shear behavior of sand under monotonic and cyclic loading and its elastoplastic modeling. 10th International Conferences on Computer Methods and Advances in Geomechanics; 2001 Jan 7-12; Arizona: USA; 2001.

[5] Benedetto HD, Doanh T, Geoffroy H, Sauzeat C. Deformation Characteristics of Geomaterials/Comportement Des Sols Et Des Roches Tendres. 1st ed. Florida: CRC Press; 2003.

[6] Phusing D and Suzuki K. Cyclic behaviors of granular materials under generalized stress condition using DEM. J Eng Mech.2015;141(10):04015034.

[7] Cundall PA, and Strack ODL. A discrete numerical model for granular assemblies. Geotechnique. 1979;29(1):47-65.

[8] Sazzad M, and Suzuki K. Density dependent macro-micro behavior of granular materials in general triaxial loading for varying intermediate principal stress using DEM. Granular Matter. 2013;15(5):583-593.

[9] Jiang M, Zhang A, Li T. Distinct element analysis of the microstructure evolution in granular soils under cyclic loading. Granular Matter. 2019;21(2):1-16.

[10] Kuhn MR. OVAL and OVALPLOT: Programs for analyzing dense particle assemblies with the discrete element method [Internet]. 2006 [cited 2021 Jun 14]. Available from: http://faculty.up.edu/kuhn/oval/doc/oval_0618.pdf).

[11] Sazzad M, Suzuki K, Modaressi-Farahmand-Razavi A. Macro-micro responses of granular materials under different b values using DEM. Int J Geomech. 2011;12(3):220-228.

[12] Rothenburg L, Kruyt NP. Critical state and evolution of coordination number in simulated granular materials. Int J Solids Struct. 2004;41(21):5763-5774.

[13] Sitharam TG. Discrete element modelling of cyclic behaviour of granular materials. Geotech. Geol Eng. 2003;21(4):297-329.

[14] Vermeer PA. Deformation and Failure of Granular Materials. 1st ed. Delft, the Netherlands. 1982.

[15] Antony SJ, Momoh RO, and Kuhn MR. Micromechanical modelling of oval particulates subjected to bi-axial compression. Comput Mater Sci. 2004;29(4):494-498.
[16] Ng TT. Macro- and micro-behaviors of granular materials under different sample preparation methods and stress paths. Int J Solids Struct. 2004;41(21):5871-5884.
[17] O'Sullivan, C., Cui, L., and O'Neil, Stuart C. Discrete element analysis of the response of granular materials during cyclic loading. Soils Found. 2008;(48):511-530.
[18] Hu M, O'Sullivan C, Jardine R, Jiang M. Stress-induced anisotropy in sand under cyclic loading. Granular Matter: 2010;12(5):469-476.
[19] Ng TT, and Dobry R. Numerical simulation of monotonic and cyclic loading of granular soil. J Geotech Eng. 1994;120(2):388-403.
[20] Phusing D, Suzuki K, and Zaman M. Mechanical behavior of granular materials under continuously varying b values using DEM. Int J Geomech. 2015;16(1):04015027.
[21] Kuhn MR, Renken HE, Mixsell AD, Kramer SL. Investigation of cyclic liquefaction with discrete element simulations. J Geotech Geoenviron Eng. 2014;140(12);04014075.
[22] Chen, Wen-Bo & Liu, Kai & Weiqiang, Feng & Yin, Jian-Hua. Partially drained cyclic behaviour of granular fill material in triaxial condition. Soil Dyn. Earthq. 2020;139:106355.
[23] Otsubo M, Chitravel S, Kuwano R, Hanley KJ, Kyokawa H, Koseki J. Linking inherent anisotropy with liquefaction phenomena of granular materials by means of DEM analysis. Soils Found. 2022;62(5):101202.
[24] Ishibashi I, and Capar O.F., Anisotropy and its relation to liquefaction resistance of granular material. Soils Found. 2003;43(5):149-159.
[25] Sze H.Y, and Yang J. Failure modes of sand in undrained cyclic loading: impact of sample preparation. J Geotech Geoenviron Eng. 2014;140(1):152-169.
[26] Tatsuoka F, Ochi K, Fujii S, Okamoto M. Cyclic undrained triaxial and torsional shear strength of sands for different sample preparation methods. Soils Found. 1986;26(3):23-41.
[27] Norouzi, N, Lashkari, A. An anisotropic critical state plasticity model with stress ratio-dependent fabric tensor. Iran J Sci Technol Trans Civ Eng 2021;45(4):2577-2594.
[28] Hu N, Yu HS, Yang DS, Zhuang Pei-Zhi. Constitutive modelling of granular materials using a contact normal-based fabric tensor. Acta Geotech. 2020;15(5):1125-1151.
[29] Nakata Y, Hyodo M, Murata H, Yasufuku N. Flow deformation of sands subjected to principal stress rotation. Soils Found. 1998;38(2):115-128.
[30] Gu X, Huang M, Qian J. DEM investigation on the evolution of microstructure in granular soils under shearing. Granular Matter. 2014; 16:91-106.
[31] Jiang M, Zhang A, Fu C. 3-D DEM simulation of drained triaxial tests on inherently anisotropic granulates. Eur J Environ Civ Eng. 2018;22:37-56.
[32] Salimi MJ, Lashkari A. Undrained true triaxial response of initially anisotropic particulate assemblies using CFM-DEM. Comput Geotech. 2020;124;103509.
[33] Liu Y, Zhang D, Wu S, Yu P. DEM investigation on the evolution of fabric under true triaxial conditions in granular materials. Int J Geomech. 2020;20(8);04020110.